Convergence of the iterative process for the diagrammatic expansion as related to liquid structure and freezing

Yaakov Rosenfeld*
The James Franck Institute, The University of Chicago, 5640 South Ellis Avenue, Chicago, Illinois 60637
(Received 30 November 1990; revised manuscript received 8 March 1991)

The stability of the solution of the hypernetted-chain (HNC) integral equation for the pair-correlation function of the fluid, with respect to its defining diagrammatic iteration loop, is investigated in one, two, and three dimensions for the inverse-power potentials characterized by a single dimensionless coupling parameter Γ. The Onsager limit and the solution of the HNC equation belong to the same basin of attraction with respect to the diagrammatic iterative map. A connection is established between (1) convergence properties of the diagrammatic low-density Mayer expansion, (2) the asymptotic strong-coupling, $\Gamma\rightarrow\infty$ ("Onsager") limit of the HNC integral equation, and (3) the freezing density of simple liquids.

I. INTRODUCTION

The exact diagrammatic description of the liquid pair structure can be cast in the form of an iteration loop, with the Mayer f bond as the initial seed.[1] Provided that the iteration procedure converges, then the corresponding sum of an infinite number of diagrams is equivalent to the solution of an integral equation, the so-called hypernetted-chain (HNC) equation, for an effective potential.[1,2] The HNC and other integral-equation methods, originating from the diagrammatic low-density expansion in terms of the Mayer f bond, have led to many advances in the theory of liquids.[2,3] The major, present day, approximate theories of the structure and thermodynamics of simple liquids have been shown[4] to interpolate between the "ideal gas" and the "ideal liquid" limits. The asymptotic limit of the hypernetted-chain integral equation (denoted the "Onsager limit"[4]) plays the role of the ideal liquid and has been proposed as the reference ideal state for developing a systematic theory of liquid structure.[4]

The present work provides a demonstration of the role of the ideal liquid (Onsager state) in the diagrammatic context; it is the starting point for a rapidly convergent high-density expansion route to liquid structure. The stability of the solution of the HNC integral equation, with respect to the original defining diagrammatic iteration loop, is investigated in one, two, and three dimensions ($D=1,2,3$) for the inverse-power potentials, $\beta\phi(r)=\Gamma r^{-m}$, characterized by a single dimensionless coupling parameter Γ. A connection is established between (1) convergence properties of the diagrammatic low-density Mayer expansion, (2) the asymptotic strong-coupling, $\Gamma\rightarrow\infty$ Onsager limit of the HNC integral equation, and (3) the freezing density of simple liquids. It is demonstrated that the Onsager limit and the solution of the HNC equation belong to the same basin of attraction with respect to the diagrammatic iteration loop. Specifically, it is found that for $\Gamma<\Gamma_C$ staring with the Onsager limit as the seed, the original diagrammatic iteration loop converges to the solution of the HNC equation. The "instability" parameters Γ_C represent an upper bound for the radius of convergence of the diagrammatic, small-Γ, Mayer expansion of the pair-correlation functions. For $\Gamma>\Gamma_C$ starting from the Onsager seed or from (arbitrarily close to) the solution to the HNC equation, the diagrammatic iteration loop converges to a limit cycle composed of several functions, the number of which generally depends on the coupling parameter Γ, the power m, and the dimensionality D. In the immediate vicinity of Γ_C, however, the limit cycle for $\Gamma>\Gamma_C$ exhibits *universal* characteristics. The instability parameters Γ_C correlate well with the freezing parameters Γ_F for these systems as obtained from computer simulations as well as with one-phase Lindemann-type freezing criteria. Monitoring the potential energy integral or the HNC free energy functional at each iteration step, it is found that the diagrammatic iteration loop for $\Gamma<\Gamma_c$ starting from the Onsager seed follows an almost monotonic path towards an energy extremum.

In Sec. II the diagrammatic expansion iteration loop is outlined, while Sec. III complies relevant properties of the ideal-liquid state. The computational setup is described in Sec. IV. The results are summarized in Sec. V and are discussed in Sec. VI. The Appendix provides the Onsager seeds used in the present study.

II. DIAGRAMMATIC EXPANSION ITERATION LOOP

The classical direct $[\phi(r)\rightarrow S(k)]$ and inverse $[S(k)\rightarrow\phi(r)]$ problems for liquid pair structure, relating the structure factor $S(k)$ to the interaction pair potential $\phi(r)$, have been reduced by exact diagrammatic analysis[1] to the solution of the HNC integral equation for an effective potential $\phi_{\rm eff}(r)=\phi(r)+B(r)/\beta$, where β is the inverse temperature $\beta=(k_BT)^{-1}$. The HNC equation is composed of the Ornstein-Zernike relation between the direct correlation function $c(r)$ and the radial distribution function $g(r)\equiv h(r)-1$ and the HNC closure. The HNC integral equation for a potential $\phi(r)$ can be written in the "series-parallel" diagrammatic iteration-loop

form.[1,2] Recalling the screening potential $H(r)=h(r)-c(r)$, the Ornstein-Zernike relation $\tilde{h}(k)=\tilde{c}(k)+\rho\tilde{h}(k)\tilde{c}(k)\equiv S(k)\tilde{c}(k)$ has the following k-space form:

$$\tilde{H}(k)=\rho\tilde{c}^2(k)/[1-\rho\tilde{c}(k)] , \quad (1)$$

representing the sum of all possible nodal diagrams obtained from diagrams in $c(r)$ by series connection. The HNC closure for a potential $\phi(r)$,

$$c(r)=\exp[-\beta\phi(r)+H(r)]-1-H(r) , \quad (2)$$

represents parallel connections of graphs in $H(r)$. ρ is the number density, and tildas denote Fourier transforms. The bridge function $B(r)$ may be expanded in diagrams with the $h(r)$ bond.[1] The assumption $B(r)=0$, i.e., $\phi_{\text{eff}}(r)=\phi(r)$, defines the HNC approximation.

The diagrammatic expansion corresponding to the HNC approximation is obtained by the following iteration loop: Starting with the Mayer f bond seed, $c_{\text{Mayer}}(r)=f(r)\equiv\exp[-\beta\phi(r)]-1$, in Eq. (1), the resulting $H(r)$ is fed into Eq. (2), which yields the first iteration for $c(r)$, which is then fed again into Eq. (1), and so on. The diagrammatic low-density expansion represents a very slowly convergent route for obtaining meaningful results for a highly correlated system like a dense fluid. Indeed, even the numerical methods for solving the HNC integral equation, although involving iteration methods, do not strictly adhere to the original diagrammatic expansion. Specifically, combined "relaxation" and "Newton-Raphson" methods of solution are employed.[5] The original diagrammatic iteration loop, without employing relaxation methods that mix input and output at each iteration step, is not considered to be a practical method for solving the equation at high densities, even if this iteration begins very close to the desired solution. Yet almost by definition, the solution by any of the numerical methods is considered complete only when two consecutive iterations of the defining (i.e., diagrammatic) interaction process are close enough.

In contract to the original diagrammatic iteration process, the HNC approximation as embodied by the solutions to the *integral equation,* provides an excellent point of departure for describing liquid pair structure.[2–4] Along this route, a first-order improvement on the HNC approximation, the ansatz of the universality of the repulsive short-range structure of $B(r)$ was found empirically to be very accurate.[2–4] It provides the key to the most successful currently available solutions of the "scattering problem."[2–4] What then is the relation, for a dense fluid, between the solution of the HNC integral equation and the diagrammatic density expansion from which this equation is derived?

III. THE ONSAGER (IDEAL LIQUID) LIMIT

Making the single assumption that the bridge function is not singular, the high-density properties of the HNC *equation* for $\phi(r)$ and $\phi_{\text{eff}}(r)$ were recently investigated.[4] The asymptotic high-density properties of the HNC equation are mapped on the Onsager lower bound to the potential energy, which features pseudoatoms and pseudomolecules as mathematical constructs. The confined-atom (*adhoc*) Thomas-Fermi theory, which provides the working hypothesis for treating very dense matter, thus corresponds to a limit of the HNC equation for classical plasmas. For a one-component plasma (OCP), i.e., positive ions in a uniform background of electrons, the Onsager lower bound corresponds to the sum of the self-energies of the neutral Onsager-Thomas-Fermi atoms each composed of a point ion at the center of a sphere of uniform negative charge density. The corresponding asymptotic HNC direct correlation functions $c^{\infty}_{\text{HNC}}(r)$ are given by the electrostatic interaction between the two uniform spheres as a function of their separation r. The Onsager lower bound for charge-cluster plasmas features Onsager "molecules" that are direct generalizations of the "atoms." This asymptotic HNC Onsager "state" provides the starting point for analyzing the structure of dense fluids (an "ideal liquid")–like the "ideal-gas" reference state for dilute fluids. This reference state involves mathematical constructs (i.e., liquidlike basis functions) that enable analytic connection to functions described by low-order diagrams.[6] The leading high-density form of $B(r)$ was derived and its universal characteristics were determined.[4]

For inverse-power potentials $\beta\phi(r)=\Gamma r^{-m}$, the asymptotic (Onsager) direct correlation function has the form $c^{\infty}_{\text{HNC}}(r)=-\Gamma\Psi(r)$, where $\Psi(r)=r^{-m}$ for $r\geq 2$, with r measured in units of the Wigner-Seitz radius a_{WS}. In these units $[\rho(a_{\text{WS}})]^D=3/4\pi,\ 1/\pi,\ \frac{1}{2}$, respectively, for $D=3,\ 2,\ 1$, so that Eqs. (1) and (2) manifestly depend only on the single parameter Γ. The Onsager-HNC function $\Psi(r)$ is available exactly for the Coulomb potential, while for other inverse-power potentials it can be well approximated, for ≤ 2, by a low-order polynomial whose coefficients are fitted to known properties of these continuous functions.[4] The present results were obtained with the functions $\Psi(r)$ given in the Appendix. Alternatively, given a numerical solution $c(r)$ to the HNC equation by any standard method at a reasonably large Γ, then one can employ (for that same power m) the function Ψ obtained by $c(r)/\Gamma$.

The present investigation was initially focused on demonstrating that the asymptotic Onsager HNC direct correlation function should somehow play the role of the Mayer f function in a high-density diagrammatic expansion. The investigation ended up finding that these asymptotic properties of the HNC equation govern its behavior in the entire fluid domain, and that at least computationally the Onsager seed performs better than the Mayer seed even in the low-density limit.

IV. COMPUTATIONAL SETUP

The computational setup, as governed by a numerical fast-Fourier-transform (FFT) procedure, is completely characterized by the mesh points for describing the correlation functions[5] $\{h(r_i);\ r_i=i\Delta r),\ i=1,\ldots,N,\ N=2^M\}$, $\{\tilde{h}(k_i);\ k_i=i\Delta k,\ \Delta k=\pi/N\Delta r\}$. The two independent parameters M and Δr were widely varied, and it was found that all the reported results are very *robust* with respect to the mesh of points, as long as enough features

of the pair correlations can still be described. A good rule of thumb is to choose $\Delta k \cong \pi \Delta r$, which yields $\Delta r \cong 1/\sqrt{N}$. Most of the qualitative results can be still exhibited for $M=6$ (i.e., $N=64$) with $\Delta r=0.125$ or $\Delta r=0.2$. This robustness enabled performance of the present study on microcomputer. A good compromise turned out to be $N=128$ with $\Delta r=0.1$ (at a rate of about 30 iterations per minute on a standard Macintosh Plus computer). The mesh size N defines the dimensionality of the iteration map. The analysis of the eigenvalues of the $N \times N$ Floquet matrix,[7] corresponding to the linear stability analysis of the map, may be greatly facilitated by a reasonably small N. A copy of the simple FORTRAN program for performing the iterations can be obtained from the author. This research was made possible by an efficient, commercial, graphics routine which almost eliminated the need to look at numerical tables. The next stage of this study requires, however, the use of a supercomputer and much work, both numerical and analytic, is required in order to fully uncover the properties and meaning of the multidimensional iterative maps as represented by the diagrammatic expansion.

The study began for the $D=3$ Coulomb potential ($m=1$), for which also the most extensive numerical results were obtained. Then other inverse powers, $m=4,6,9,12$, were extensively studied for $D=3$. The calculations for $D=2$ and $D=1$ were extensive enough to establish qualitative results, but a supercomputer is needed to obtain more accurate estimates of Γ_C. Some of our results for the Coulomb potential (OCP) were independently reproduced[8] upon our request to further eliminate the possibility of a systematic error.

At any given iteration step, we found it useful to define and monitor the following quantities: at the "series" part of the loop, i.e., Eq. (1), define $h_S(r)$ as the inverse Fourier transform of $\tilde{h}_S(k) \equiv \tilde{c}(k)/[1-\rho\tilde{c}(k)]$, and in the parallel part of the loop, i.e., Eq. (2), define $h_P(r) \equiv \exp[-\beta\phi(r)+H(r)]-1$. For physically allowed $\tilde{c}(k)$, we must have $1+\rho\tilde{h}_S(k) \geq 0$, while for physically allowed $H(r)$ we must have $1+h_P(r) \geq 0$. A physically acceptable solution of the HNC equation must in addition satisfy $h_P(r)=h_S(r)$ (to within the prescribed numerical accuracy). At any given iteration step define u_P and u_S, the potential-energy integrals, as obtained from

$$u=(\rho/2)\int [h(r)+1]\beta\phi(r)d\mathbf{r} ,$$

upon using $h_P(r)$ and $h_S(r)$, respectively. For the OCP use $h(r)$ instead of $h(r)+1$ in the integral. We similarly monitored the corresponding expressions for the HNC free energy integrals.[4] Our computer program is constructed to perform the diagrammatic iteration loop. Eqs. (1) and (2), as is, in addition, we have the option to run the program with the standard mixing procedure (the relaxation method) as a means to obtain a "brute-force" solution to the integral equation to any desired numerical accuracy.

V. RESULTS

Given the power m and the dimensionality D the following two types of calculations were performed as a function of the coupling parameter Γ. (i) Starting with the Onsager seed $c_O(r)=-\Gamma\Psi(r)$, generate a number of iterations n_{diag} of the diagrammatic iteration loop. (ii) Starting with the Onsager seed generate a mixing iteration loop to obtain an accurate solution (accuracy depending on the number n_{mix} of such iterations), and then starting with this solution to the HNC equation as the seed, generate a number n_{diag} of the diagrammatic iteration loop. Depending on the case for either type-(i) or

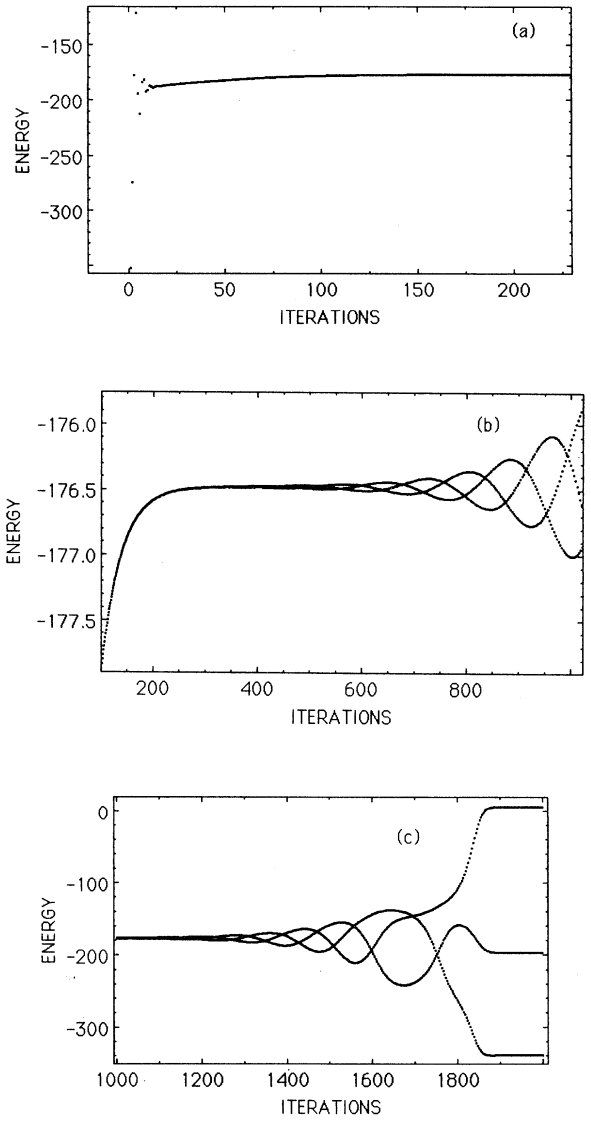

FIG. 1. The one-component plasma ($m=1$, $D=3$) potential energy (u_P, see the text) as a function of the iteration using a mesh of 128 points with $\Delta r=0.1$ for $\Gamma=203$. Starting with the Onsager seed, two diagrammatic iterations followed by 50 mixing iterations and continuing with diagrammatic iterations. See the text. Note how first the iterations converge to a single function and then they eventually reach the limit cycle (compare with Fig. 2).

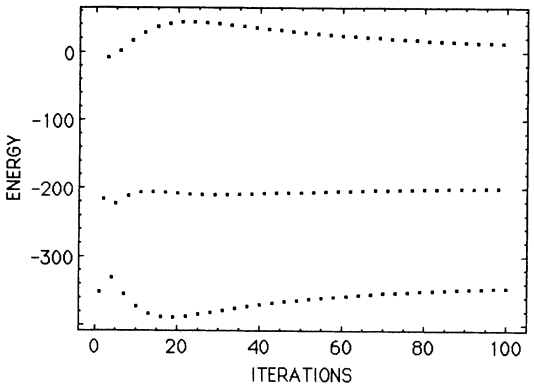

FIG. 2. The one-component plasma ($m=1$, $D=3$) potential energy (u_P, see the text) as a function of the iteration number, for the diagrammatic iteration loop with the Onsager seed using a mesh of 128 points with $\Delta r=0.1$ for $\Gamma=203$. See the text and compare with Fig. 1.

type-(ii) calculations, n_{mix} could reach several hundred iterations, while n_{diag} reached up to several thousand (in which case a faster microcomputer, Macintosh SE/30, was employed).

The general main result of the present extensive numerical study is that provided $n_{\text{diag}} \gg n_{\text{mix}}$, the end results of these two types of calculations are essentially the same. In other words, the Onsager limit and the solution to the HNC equation belong to the same basin of attraction with respect to the diagrammatic iterative map. The significance of the ideal-liquid state in the diagrammatic context can be also appreciated as follows: The Onsager ideal-liquid limit provides a very efficient and sensitive probe for the stability of the HNC solution with respect to the diagrammatic iterations. In Fig. 1 we see directly how long it takes for a nearly convergent solution to "unwind" in a type-(ii) calculation, while the end pattern of the iterations is immediately seen in the corresponding type-(i) calculation (Fig. 2). In general, the larger the n_{mix} (i.e., the closer one gets to the solution), the larger the n_{diag} required in the type-(ii) calculation in order to see the pattern which, in turn, was almost immediately seen (with a rather small n_{diag}) in the corresponding type-(i) calculation.

Subject to this general observation, the following general results were obtained from the type-(i) calculation, namely with the Onsager seed in the diagrammatic iteration loop.

(i) For *all* $\Gamma<\Gamma_C$ the calculations always converge to the solution of the HNC integral equation. A list of estimates of Γ_C is given in Table I where they are compared with the freezing parameters.[9] The instability parameters Γ_C were estimated as follows. For relatively small Γ the diagrammatic iteration loop quickly converges to the solution of the HNC equation. Increasing the value of Γ and repeating the type-(i) calculation, the iterations begin to feature a three-function cycle which slowly converges

TABLE I. Instability coupling parameters Γ_C as compared with the freezing Γ_F and melting Γ_M values[9] as well as with a structural freezing criterion (Ref. 9) given by $\Gamma_G\cong(50/\alpha)/A(m/D)$, where $A(x)=x(x+1)-4(1-2^{-x})$, and α is the HNC Madelung constant ($\alpha=u/\Gamma$ for large Γ). The values for Γ_C are based on results for meshes of 128 and 256 points (see the text).

Dimensionality D	Power m	Γ_C	Γ_F	Γ_M	Γ_G
3	1	198±2	180	180	146
	4	74±2	66	67	61
	6	91±2	83	85	84
	9	179±2	174	190	220
	12	440±5	541	625	786
2	1	80±5			107
	3	45±5			45
	6	55±5			59
	8	85±5			74
1	−1	70±2			75
	2	25±2			41
	4	25±5			56

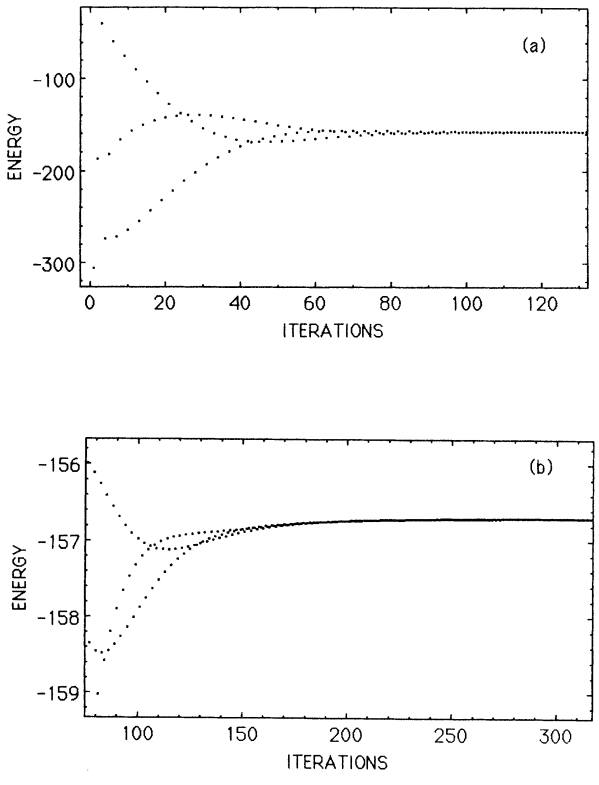

FIG. 3. The one-component plasma ($m=1$, $D=3$) potential energy (u_P, see the text) as a function of the iteration number for the diagrammatic iteration loop with the Onsager seed using a mesh of 128 points with $\Delta r=0.1$ for $\Gamma=180$.

to the solution. For a slightly larger value of Γ the amplitude of the three-function cycle pattern persists (see below) indefinitely, i.e., the iteration process quickly reaches a limit cycle. For example, the three-function limit cycle results for $\Gamma=180,197,198$ for the OCP ($m=1$) in three dimensions are presented in Figs. 3–5. For the $D=3$ OCP we find that for both $N=128$ and $N=256$, Γ_C is located between 197 and 198, while for $N=64$, Γ_C is between 196 and 197. As one comes closer to Γ_C the sensitivity of the iteration loop to perturbations increases. Figure 6 represents the results for the case of Fig. 5 but with five mixing iterations before the diagrammatic loop begins. The possible accuracy for determining Γ_C depends on the Liapunov exponent for the type of convergence exhibited in Fig. 4(b). The error bars in Table I essentially reflect the limitations of a microcomputer. It is to be noted, however, that meaningful improvement requires a supercomputer.

(ii) As the iteration number increases for $\Gamma<\Gamma_C$ the energy integral u_S is generally monotonically decreasing while the energy integral u_P is monotonically increasing, and eventually they become equal for the HNC solution (Fig. 7). This behavior of the diagrammatic iteration loop, featuring the solution as both a minimum and a maximum depending on boundary conditions for the structure functions, has already been encountered[4] for the Onsager limit. The Onsager limit can be obtained as a "best lower bound problem," i.e., seeking a maximum, and as a "lowest self-energy problem," i.e., seeking a minimum.[10] It is remarkable that the Onsager best-

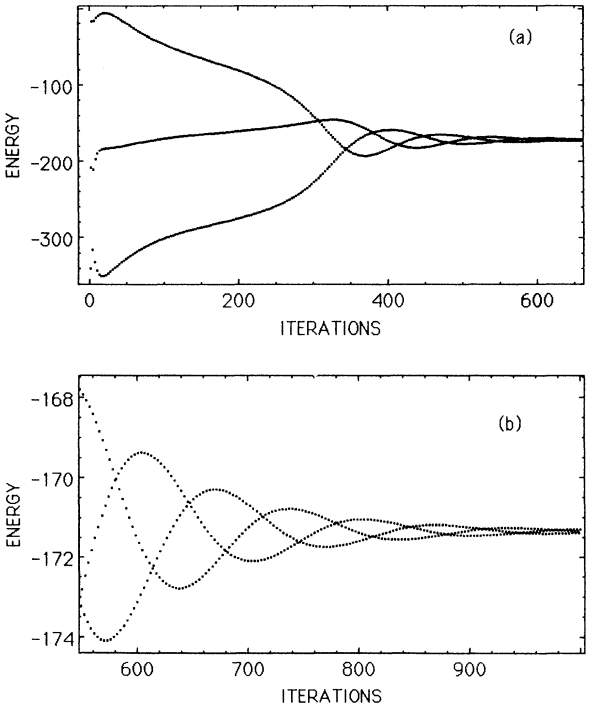

FIG. 4. Same as Fig. 3 but for $\Gamma=197$.

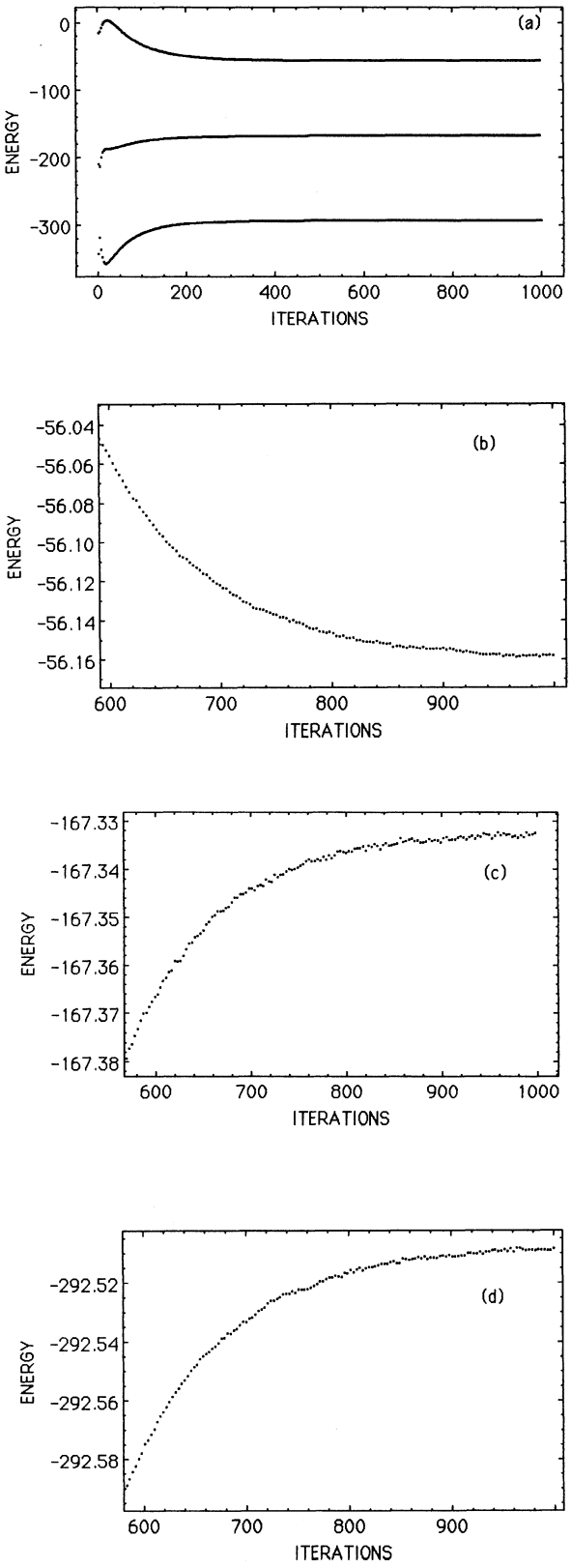

FIG. 5. Same as Fig. 3 but for $\Gamma=198$.

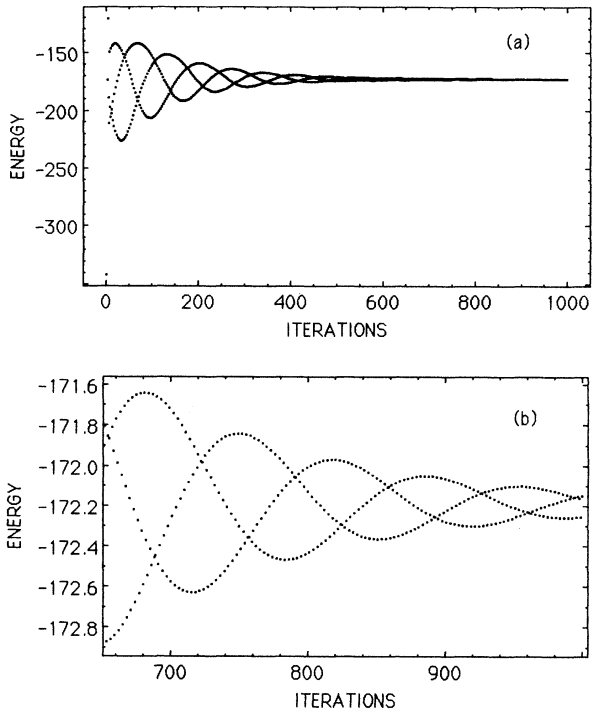

FIG. 6. Same as Fig. 5 starting with the Onsager seed, then two diagrammatic iterations followed by five mixing iterations, and continuing with diagrammatic iterations. See the text.

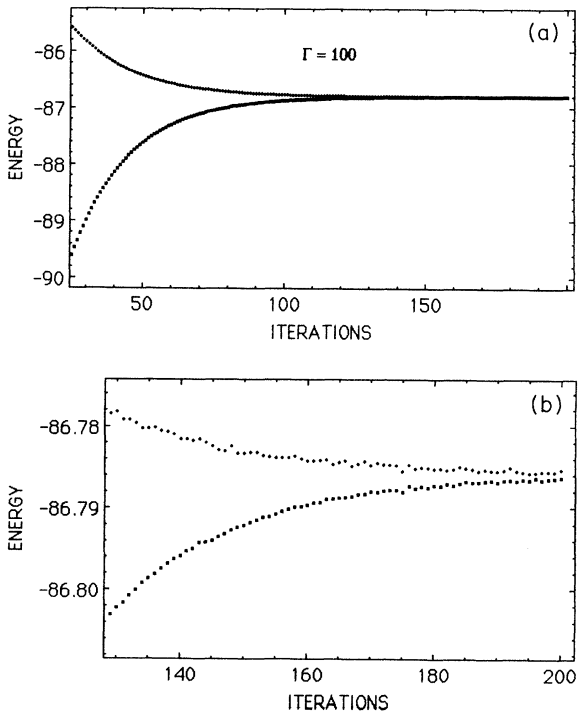

FIG. 7. The one-component plasma ($m=1$, $D=3$) potential energy (u_S and u_P, see the text) as function of the iteration number for the diagrammatic iteration loop with the Onsager seed using a mesh of 128 points with $\Delta r=0.1$, for $\Gamma=100$. Panel (b) is an enlargement of the energy region $-86.81 \lesssim u_{S,P} \lesssim -86.77$.

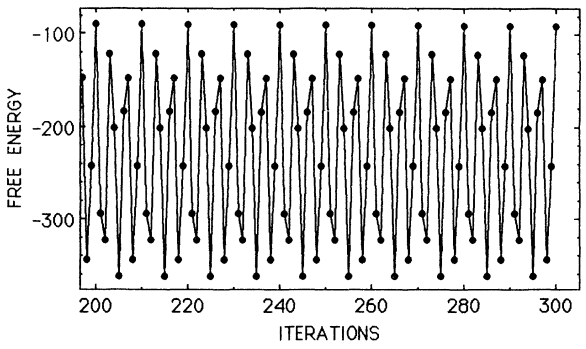

FIG. 8. The HNC free energy for the one-component plasma ($m=1$, $D=3$) as a function of the iteration number, displaying a ten function limit cycle for $\Gamma=280$. See the text and the caption to Fig. 7.

lower-bound problem represents the asymptotic limit of the HNC variational problem constrained by positive definite $S(k)$, while the Onsager lowest-self-energy problem represents the asymptotic limit of the HNC variational problem constrained by positive definite $g(r)$.

(iii) For $\Gamma > \Gamma_C$ starting from the Onsager seed the diagrammatic iteration loop rapidly converges to a limit cycle composed of several functions, the number of which may depend on the coupling parameter Γ, the power m, and the dimensionality D. An example of a ten-function limit cycle is presented in Fig. 8. Other and more complex patterns occur also, as expected from a multidimensional nonlinear iterative map.

In the vicinity of Γ_C, however, and for $\Gamma > \Gamma_C$, the iterations *always* begin to exhibit a three-function cycle pattern. These three-function patterns gradually change (for example, Fig. 4) as the iterations continue. Considering the time series $E(t)$, i.e., the energy versus iteration number, as displayed in the figures, then $E(t)$ seems to converge for $\Gamma > \Gamma_C$ to a pattern $E^{(\infty)}(t)$ that can be expressed by the following *universal* form:

$$E=E^{(\infty)}(t)=F(t-L(t \bmod 3)) \quad \text{for } t \gg 1 \, . \tag{3}$$

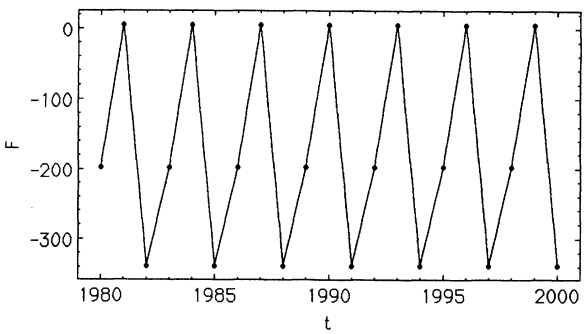

FIG. 9. Periodic function $F(t)$ corresponding to the energy vs iterations of Fig. 2. See the text.

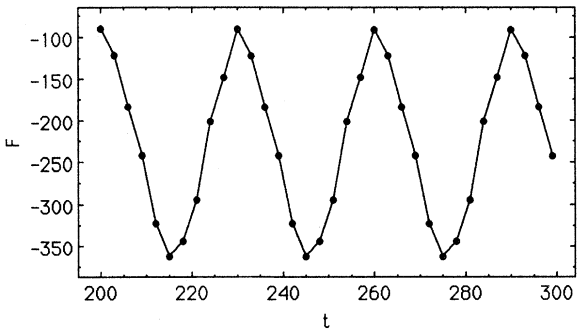

FIG. 10. Periodic function $F(t)$ corresponding to the energy vs iterations of Fig. 8. See the text.

The function $F(t)$ is periodic with period $\mathcal{T}$. The number of functions in the limit cycle N_E, i.e., the number of distinct energy levels in the pattern $E^{(\infty)}(t)$, satisfies $N_E \leq L$. For example, Figs. 1 and 2 correspond to $\mathcal{T}=3$, $L=3$, $N_E=3$, with the function $F(t)$ given in Fig. 9, while Fig. 8 corresponds to $\mathcal{T}=30$, $L=N_E=10$, with the function $f(t)$ given in Fig. 10. The cases $m=1$ in two and three dimensions ($D=2,3$) are the only cases we studied to feature $L=3$ in the immediate vicinity of Γ_C. An example of the three-function limit cycle is presented in Fig. 11. It should be emphasized that *none* of the functions in a multifunction limit cycle corresponds to a solution of the HNC equation. Specifically, none of these functions satisfies $h_S(r)=h_P(r)$, and in most cases $h_S(r)$ has an unphysical region. Since, in particular, the three-function limit cycles does not correspond to a trifurcation of the ordinary solution, its relation (if any) to the Hammerstein-type integral equation analysis[11] remains to be clarified. Other inverse power potentials in general as well as the one-component plasma ($m=-1$) in one dimension exhibit $N_E \gg 1$, with $\mathcal{T}=3L$ as given, for example, by Figs. 12 and 13, which should be compared with Figs. 1 and 2. The three-function limit cycle for the OCP ($m=1$) persists in $D=3$ up to about $\Gamma=230$, where it gives room to a multifunction limit cycle. Compare Figs. 14 and 15, both describable by Eq. (3). The value of L at

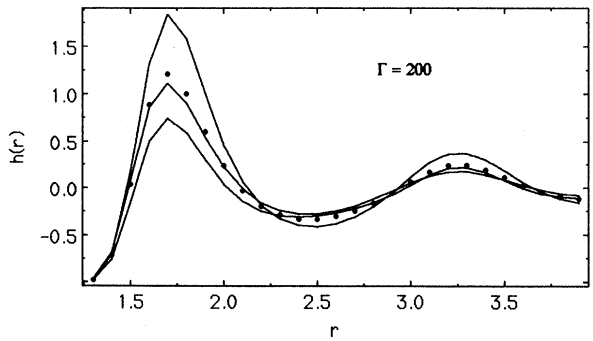

FIG. 11. The three-function limit cycle [the functions $h_P(r)+1$, see the text] for the one component plasma ($m=1$, $D=3$) at $\Gamma=200$, compared with the solution to the HNC equation (closed circles). See caption to Fig. 7.

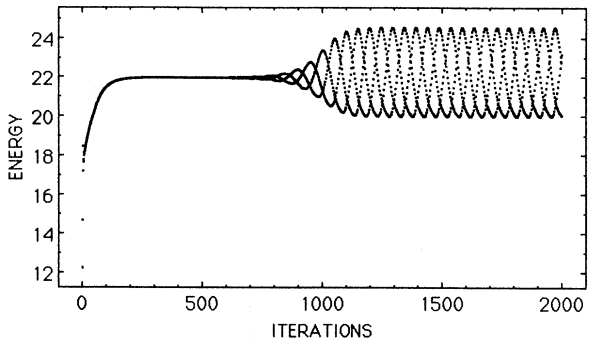

FIG. 12. Same as Fig. 1 but for $m=6$, $D=3$, $\Gamma=92$.

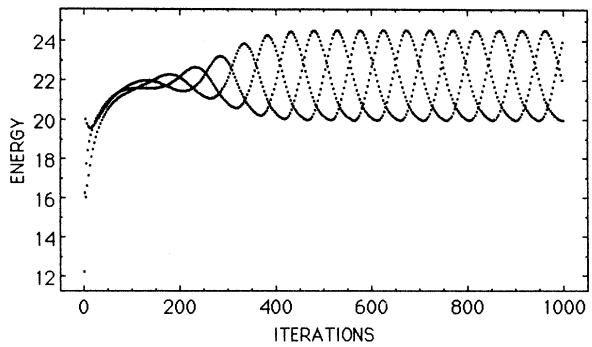

FIG. 13. Same as Fig. 2 but for $m=6$, $D=3$, $\Gamma=92$.

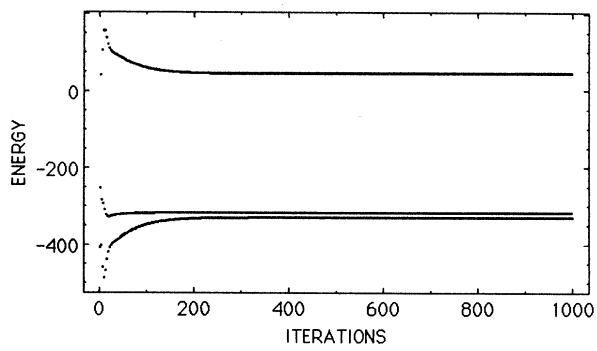

FIG. 14. Same as Fig. 3 but for $\Gamma=230$.

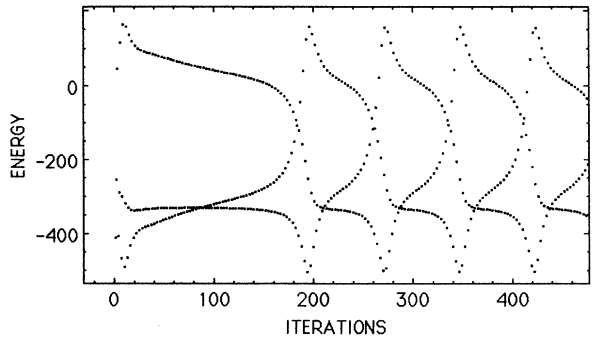

FIG. 15. Same as Fig. 3 but for $\Gamma=232$.

Γ_C is a decreasing function of the power m for fixed D. Except for the initial increase of L for the cases featuring $L=3$, in general L is then a decreasing function of Γ, in the immediate vicinity of Γ_C, for fixed m and D.

VI. DISCUSSION

The relevant scale for evaluating the correlations between the instability parameters Γ_C and freezing is the density change upon freezing. On this scale, the instability parameters Γ_C correlate well with the freezing parameters Γ_F for the corresponding systems as obtained from computer simulations in $D=3$, as well as with one-phase Lindemann-type structural freezing criteria (for example, Γ_G) in $D=1,2,3$. Note that the structural criterion for freezing Γ_G is expected to be at least as accurate in $D=2$ as in $D=3$. Being a structural Lindemann-type and not a thermodynamic freezing criterion, Γ_G can be meaningfully evaluated also in $D=1$. Since the diagrammatic iteration proceed without input about characteristics of the solid, Γ_C cannot be equal to Γ_F and thus represents a structural freezing indicator.

The type-(i) calculation starts with the Onsager seed, $c_O(r)=-\Gamma\Psi(r)$, which is inserted into an "unmixed" diagrammatic iteration loop. Thus, for a given power potential *it depends only on the physical coupling parameter* Γ. The instability parameters Γ_C represent an upper bound for the radius of convergence of the diagrammatic, small-Γ, Mayer expansion of the pair-correlation functions. The strong correlation between Γ_C and freezing, which should be judged on the scale of typical differences between Γ_F, Γ_M, and Γ_G, demonstrates that the diagrammatic iteration process, which eventually builds up the fluid correlation functions, also contains information regarding the stability of this structure. Specifically, the type-(i) calculation yields the HNC solution, which is a nontrivial reasonably accurate description of the OCP fluid pair structure, and without any outside intervention it "rings a bell" at Γ_C, which is close to Γ_F. It is interesting to note in Table I for $D=3$ that $\Gamma_C>\Gamma_M$ for $m\leq 6$, while $\Gamma_C<\Gamma_M$ for $m>6$. A remote possibility is that this feature might be related to the simulation results, in which, for $m\gtrsim 7$, the inverse-power potential liquid freezes into a fcc crystal structure, while for $m\lesssim 7$, the bcc structure becomes the equilibrium freezing solid structure. Further analysis of the diagrammatic iteration process, using new methods recently developed for studying iterative maps,[7] can reveal characteristics of the liquid structure that are relevant for its relative stability. Even the linear-stability analysis of the map may lead to an alternative quantitative structural definition for effective packing. Finally, the present results indicate that the recent attempts[12] to characterize supercooled liquids and glasses by the solution of the HNC equation for semiempirical bridge function $B(r)$ must proceed with caution.

ACKNOWLEDGMENTS

Interesting discussions with David Oxtoby and Stuart Rice are acknowledged with gratitude. I also thank Fred Lado, Dominique Levesque, and Jean-Jacques Weis for helpful correspondence.

APPENDIX: ASYMPTOTIC DIRECT CORRELATION FUNCTIONS

For inverse-power potentials $\beta\phi(r)=\Gamma r^{-m}$ the asymptotic (Onsager) direct correlation function has the form $c^{\infty}_{\rm HNC}(r)=-\Gamma\Psi(r)$, where $\Psi(r)=r^{-m}$ for $r\geq 2$, with r measured in units of the Wigner-Seitz radius, $a_{\rm WS}$. The asymptotic function $\Psi(r)$ is conveniently described by the corresponding Onsager-Ewald function $f(t)$, as follows:[4]

$$\Psi(r)=r^{-m}[1/W(m)]\int_0^{r/2} f(t)t^{m-1}dt \ , \tag{A1}$$

where

$$W(m)=\int_0^{\infty} f(t)t^{m-1}dt \ . \tag{A2}$$

In addition to other properties,[4] $f(t)$ must satisfy

$$f(t\geq 1)=0 \ , \tag{A3a}$$

$$f(t)\geq 0 \ , \tag{A3b}$$

$$DW(m=D)=2^{-D} \ . \tag{A3c}$$

Only the hard-sphere and Coulomb-Ewald functions are known exactly. The $D=1$ and $D=3$ hard-sphere functions are

$$f(t\leq 1)=\begin{cases}1-t & \text{for } D=1 \qquad \text{(A4a)}\\ 1-1.5t+0.5t^3 & \text{for } D=3 \ . \qquad \text{(A4b)}\end{cases}$$

The $D=1$ and $D=3$ Coulomb functions are

$$f(t\leq 1)=\begin{cases}1-3t^2+2t^3 & \text{for } D=1 \qquad \text{(A5a)}\\ 1-5t^2+5t^3-t^5 & \text{for } D=3 \ . \qquad \text{(A5b)}\end{cases}$$

In the present study we used for $D=2$ the following Ewald function for all powers of m:

$$f(t)=x(1-3t^2+2t^3)+(1-x)(1-5t^2+5t^3-t^5) \ , \tag{A6}$$

where $x=\frac{5}{12}$ is obtained from (A3c). For $D=1$ and 3 we use an interpolation between the hard-sphere and Coulomb functions:

$$f(t)=\begin{cases}x(1-t)+(1-x)(1-3t^2+2t^3) & \text{for } D=1\\ x(1-1.5t+0.5t^3)+(1-x)(1-5t^2+5t^3-t^5) & \text{for } D=3 \ ,\end{cases} \tag{A7}$$

(A8)

where for each power of m, x is obtained from the known HNC Madelung constant ($\alpha=u/\Gamma$ for large Γ), related to the Onsager-Ewald $f(t)$ by

$$\alpha(m)=D2^{-m}/[2m(m-D)W(m)] . \quad \text{(A9)}$$

For $D=1$ we have $\alpha(m)=2^{-m}\zeta(m)$, where ζ is Riemann's zeta function. For $D=3$, using the table in Ref. 4(b) we find $x=0.109\,415$, $0.164\,891$, $0.234\,345$, and $0.285\,826$, respectively, for $m=4$, 6, 9, and 12. Finally, it should be emphasized that the global basin of attraction for the HNC solution is reasonably wide, and the results are not sensitive to reasonably wide variations in $f(t)$. For example, using $f(t)=\exp(-t^2)$ for the Coulomb potential leads to the same result as using the exact HNC Ewald function (A5b).

---

*Permanent address: The Nuclear Research Center–Negev, P.O. Box 9001, Beer-Sheva, Israel.

[1]J. M. J. van Leeuven, J. Groeneveld,, and J. de Boer, Physica (Utrecht) **25**, 792 (1959); T. Morita and K. Hiroike, Prog. Theor. Phys. (Jpn.) **23**, 1003 (1960).

[2]Y. Rosenfeld and N. W. Ashcroft, Phys. Rev. A **20**, 1208 (1979). This paper contains an appendix discussing the diagrammatic iteration loop for the Coulomb potential.

[3]J. A. Barker and D. Henderson, Rev. Mod. Phys. **48**, 587 (1976). J. P. Hansen and I. R. McDonald, *Theory of Simple Liquids*, 2nd ed. (Academic, London, 1986); J. Talbot, J. L. Lebowitz, E. M. Weisman, D. Levesque, and J. J. Weis, J. Chem. Phys. **85**, 2187 (1986). See also the recent review, R. Evans, in *Liquids at Interfaces*, Proceedings of the Les Houches Session No. 48, edited by J. Chavrolin, J. F. Joanny, and J. Zinn-Justin (Elsevier Science, New York, 1989).

[4](a) Y. Rosenfeld, Phys. Rev. A **32**, 1834 (1985); (b) **33**, 2025 (1986); (c) **35**, 938 (1987); (d) **37**, 3403 (1988); Y. Rosenfeld, D. Levesque, and J. J. Weis, *ibid*, **39**, 3079 (1989); (e) D. Ofer, E. Nardi, and Y.Rosenfeld, *ibid*. **38**, 5801 (1988).

[5]See, for example, M. J. Gillan, Mol. Phys. **38**, 1781 (1979); G. M. Abernethy and M. J. Gilan *ibid*. **39**, 839 (1980); S. Labik, A. Malijevsky, and P. Vonka, *ibid*. **56**, 709 (1985). An example of a $D=3$ program is K. C. Ng, J. Chem. Phys. **61**, 2680 (1974). A $D=2$ program is desribed by J. P. Hansen and D. Levesque, J. Phys. C **14**, 603 (1981). This program is based on J. D. Talman, J. Comput. Phys. **29**, 35 (1978). The more standard method for $D=2$, as described by F. Lado, J. Chem. Phys. **49**, 3092 (1968), is more time consuming and could not be used on a microcomputer.

[6]Y. Rosenfeld, J. Chem. Phys. **89**, 4272 (1988); Phys. Rev. Lett. **63**, 980 (1989); Y. Rosenfeld, D. Levesque, and J. J. Weis, J. Chem. Phys. **92**, 6818 (1990).

[7]See, for example, P. Bergé, Y. Pomeau, and C. Vidal, *Order Within Chaos* (Wiley, New York, 1986).

[8]C. Dharma-wardana and F. Perrot (private communication).

[9]Reviews of computer-simulation freezing data is given by W. G. Hoover and M. Ross, Contemp. Phys. **12**, 339 (1971); S. M. Stishov, Usp. Fiz. Nauk. **112**, 3 (1974) [Sov. Phys.—Usp. **17**, 625 (1975)]; **154**, 93 (1988) [**31**, 52 (1988)]. Structural Lindemann-type criteria are reviewed by Y. Rosenfeld, Phys. Rev. A **24**, 2805 (1981), from where Γ_G of Table I is derived.

[10]J. Stein, D. Shalitin, and Y. Rosenfeld, Phys. Rev. A **37**, 4854 (1988), Fig. 4.

[11]See, for example, the review by John J. Kozak, in *Advances in Chemical Physics*, edited by I. Prigogine and S. A. Rice (Wiley, New York, 1979), Vol. XL.

[12]See, for example, S. Kambayashi and Y. Hiwatari, Phys. Rev. A **41**, 1990 (1990), and references therein.